Journal Name

Dynamic Article Links ►

Cite this: DOI: 10.1039/c0xx00000x

www.rsc.org/xxxxxx

ARTICLE TYPE

Synthesis, structural, photophysical and electrochemical studies of various *d*-metal complexes of btp [2,6-bis(1,2,3-triazol-4-yl)pyridine] ligands that give rise to the formation of metallo-supramolecular gels†

Joseph P. Byrne,[a] Jonathan A. Kitchen,[a,d] Oxana Kotova,[a] Vivienne Leigh,[b] Alan P. Bell,[c] John J. Boland,[c] Martin Albrecht[b] and Thorfinnur Gunnlaugsson*[a]

Received (in XXX, XXX) Xth XXXXXXXXX 20XX, Accepted Xth XXXXXXXXX 20XX

DOI: 10.1039/b000000x

2,6-Bis(1,2,3-triazol-4-yl)pyridine (btp) is a terdentate binding motif that is synthesised modularly *via* the CuAAC reaction. Herein, we present the synthesis of ligands 1 and 2 and the investigation into the coordination chemistry, photophysical behaviour and electrochemistry of complexes of these with a number of *d*-metal ions (*e.g.* Ru(II), Ir(III), Ni(II) and Pt(II)). The X-ray crystal structures of ligand 1 and the complexes $[Ru{\cdot}2_2]PF_6Cl$, $[Ni{\cdot}1_2]PF_6Cl$ and $[Ir{\cdot}1Cl_3]$ are also presented, but all the complexes displayed non-classical triazolyl C–H···Cl⁻ hydrogen bonding. All but one complex showed no metal-based luminescence at room temperature, while, for example the Pt(II) complexes displayed luminescence at 77 K. The electrochemistry of the Ru(II) complexes was also studied and they were found to have higher oxidation potentials than analogous compounds. The redox behaviour of $[RuL_2]^{2+}$ complexes with both 1 and 2 was nearly identical, while $[Ru{\cdot}1Cl_2(DMSO)]$ was oxidised at significantly lower potential. We also show that the Ru(II) complex of 2, $[Ru2_2]PF_6Cl$, gave rise to the formation a metallo-supramolecular gel; the morphology of which was studied using by scanning electron and helium ion microscopy.

Introduction

Transition metal ion complexes are widely studied, particularly with respect to their photophysical properties, electrochemical properties and potential biological applications. The d^6 metal ions Ru(II) and Ir(III) and d^8 metal ions Ni(II) and Pt(II) have all shown significant applications in biological systems, as cellular imaging agents,[1,2] DNA binders[3,4] and in anti-cancer treatment,[5] but the complexes of these metals are usually kinetically inert and stable. Pyridine-centred terdentate binding motifs are a particularly privileged coordinating environment for such metal ions. For example, 2,2′:6′,2″-terpyridine (terpy) and its derivatives are ubiquitous in the literature, featuring in dye-sensitised solar cells,[6] DNA and protein binding,[3,4] metallo-supramolecular coordination polymers,[7] and in ion sensing.[8] These ligand are, however, limited by the synthetic challenge involved in derivatising them, particularly with regard to introducing flanking 'arms' appended to the non-central heterocycles. Facile and modular synthesis of such ligands is of great interest and has–in recent years–led to increased interest in the 2,6-bis(1,2,3-triazol-4-yl)pyridine (**btp**)[‡] moiety. **Btp**-based ligands can be obtained *via* the Cu(I)-catalysed alkyne–azide 'click' (CuAAC) reaction from a wide range of substrates.[9-13] The CuAAC reaction is a regioselective, high yielding and tolerant reaction that gives exclusively 1,4-disubstituted 1,2,3-triazole products.[14-18] The **btp** binding motif has been shown by Flood *et al*. to form stable coordination compounds[12] and has been utilised in such diverse applications as tuning the optical properties of Ru(II)-polypyridyl complexes,[19] in the formation of metallo-supramolecular architectures[18] and polymers,[20] binding halides,[21] sensitisation of lanthanide luminescence in the solid state[22] and recently by Yuan *et al*. [23] in the formation of self-healing metallo-supramolecular gels. Hence, **btp** is a highly versatile building block that we have recently started working with. Herein we report the synthesis of **btp** ligands **1** and **2** (**Scheme 1**) and their coordination chemistry with Ru(II), Ir(III), Ni(II) and Pt(II), as well as various structural, photophysical and electrochemical analyses of these complexes. Ru(II) complexes with polypyridyl ligands have been studied in the past with particular interest being paid to their electrochemical and photophysical properties. Bis-terdentate complexes such as $[Ru(terpy)_2]^{2+}$ overcome isomerism and provide more linear structure than tris-bidentate complexes. Zhang *et al*. showed that the **btp** motif has very similar binding properties to terpy, with similar bond angles and lengths determined by X-ray diffraction therefore making study of such systems valuable as an analogue for terpy.[24] A number of

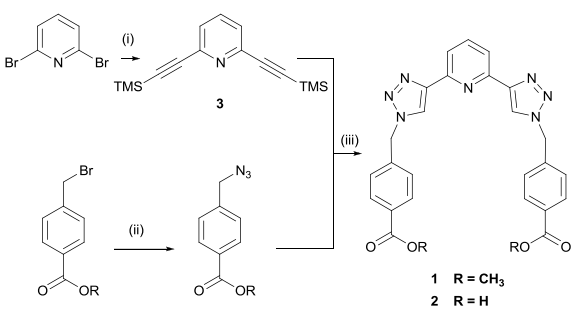

Scheme 1 Synthesis of ligands **1** and **2**. (i) CuI, $(PPh_3)_2PdCl_2$, THF/Et_3N (1:1), trimethylsilylacetylene, 0 °C→rt; (ii) NaN_3, rt, 1h, DMF/H_2O; (iii) $CuSO_4{\cdot}5H_2O$, Na ascorbate, K_2CO_3, DMF/H_2O, rt, 18h.

Ru(II) complexes with **btp** have subsequently been recently reported, showing indeed such similar characteristics to the terpy analogues.[12,19,20,25-27] However, to the best of our knowledge, there are no examples in the literature of Ir(III) complexes with **btp**-containing ligands. Giving that Ir(III) is isoelectronic to Ru(II) and its complexes have long been of interest, due to their emission properties, we decided to investigate their formation herein.[28] The d^8 octahedral Ni(II) complexes are isostructural to the octahedral d^6 metal complexes. Only one example of the interaction between the **btp** motif and the square planar d^8 Pt(II) ion has been reported, where it was used in the formation of metallopolymers.[29] The chemistry of Pt(II)-terpy derived systems is, however, well studied, often as a result of their ability to exhibit metal···metal interactions.[30,31] There have only been, to the best of our knowledge, two **btp**-based supramolecular gels previously reported in the literature. One responsive system exploited the conformational changes that **btp** undergoes upon binding a metal (*vide infra*) to interconvert between a helically folded polymer and a metallo-supramolecular cross-linked gel,[32] while the other work described self-healing polymeric materials[23]. Both of these systems involved polymeric poly-**btp** components, we herein present the first example of a metallo-supramolecular gel derived from discrete mono-**btp** components (*i.e.* ligand **2**). In this article we give full account of our results.

Results and discussion

Synthesis and characterisation

Ligands **1** and **2** were synthesised in a one-pot deprotection/'click' reaction from the relevant bromide and 2,6-bis((trimethylsilyl)ethynyl)-pyridine (**3**) where the azide was produced with subsequent alkyne deprotection *in situ*, following a paradigm used by Fletcher *et al.*[33,34] as shown in Scheme 1. Upon washing the reaction mixture with EDTA/NH_4OH solution, the ligands were obtained in high purity (confirmed by elemental analysis), which eliminated the need of any further purification (such as the use of chromatography) and moderate yields of 53% and 63%, respectively,

Due to the C_2-symmetry in both **1** and **2**, only a few resonances were observed in the ^{1}H-NMR spectra. The spectrum of **1** was recorded in both DMSO-d_6 and $CDCl_3$ solutions (both shown in ESI). The spectrum shown in **Fig. 1(a)** (400 MHz, DMSO-d_6) displayed the expected number of resonances for **1**. The triazolyl peak appeared as a well resolved singlet at 8.72 ppm (marked *t* in **Fig. 1**), a multiplet at 7.91–8.07 ppm was made up from the overlap of the pyridyl signals with one of the phenyl signals. The other resonance from the phenyl ring was observed at 7.45 ppm (marked *x*) and two singlets (*y* and *z*) at 5.81 and 3.84 ppm arose from the methylene and methyl ester moieties, respectively.

The carboxylic acid ligand **2** was found to have poor solubility in organic solvents. The ^{1}H-NMR spectrum (600 MHz, DMSO-d_6) was once again very simple (ESI **Fig. S3**). The resonance at 5.80 ppm arose from the methylene linker, a doublet at 7.45 ppm related to four of the eight phenyl CH protons, the multiplet from 7.88–8.06 ppm resulted from the overlap of the remaining phenyl signal and the two pyridyl resonances, the singlet at 8.74 ppm was related to the triazolyl protons. Having made these ligands we next formed the various *d*-metal ion complexes of **1** and **2**.

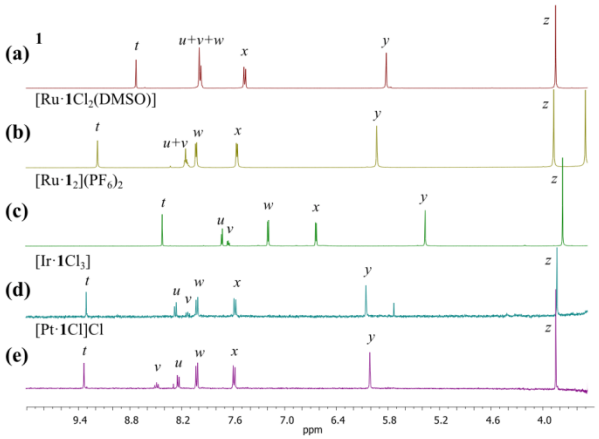

Fig. 1 Comparison of the chemical shifts of the proton resonances in ^{1}H NMR spectra of (a) Ligand **1** (400 MHz, DMSO-d_6); (b) [Ru·**1**Cl_2(DMSO)] (600 MHz, DMSO-d_6); (c) [Ru·**1**$_2$]$(PF_6)_2$ (600 MHz, DMSO-d_6); (d) [Ir·**1**Cl_3] (400 MHz, DMSO-d_6); (e) [Pt·**1**Cl]Cl (400 MHz, DMSO-d_6). Peaks are labelled as follows: *t* (triazolyl CH), *u* (3- and 5-pyridyl CH), *v* (4-pyridyl CH), *w* and *x* (phenyl CH), *y* (CH_2), *z* ($-OCH_3$).

The monoleptic Ru(II) complex of **1** was prepared upon treating ligand **1** with 1 molar equivalent of $[RuCl_2(DMSO)_4]$ in $CHCl_3$ under reflux conditions and [Ru·**1**Cl_2(DMSO)] was collected upon filtration as a bright red solid in good yield (86%). The ^{1}H-NMR spectrum (600 MHz, DMSO-d_6; **Fig. 1(b)** and shown in full in ESI, **Fig. S3**) showed resonances shifted relative to the ligand, as well as a new resonance appearing at 3.49 ppm, arising from the bound DMSO molecule in the structure. MALDI HRMS confirmed this, showing the presence of $[M-(DMSO)]^+$ species corresponding to *m/z* = 681.0213 with an isotopic distribution pattern matching the calculated one (*cf.* ESI, **Fig. S12**).

The dileptic complex [Ru·**1**$_2$]$(PF_6)_2$ was prepared upon heating 2 equivalents of ligand **1** with 1 equivalent of $RuCl_3 \cdot xH_2O$ under microwave irradiation to 120 °C for 40 minutes, and isolated by counterion exchange to the PF_6 salt. The ^{1}H-NMR spectrum (600 MHz, DMSO-d_6) is shown in **Fig. 1(c)**. The doublet and triplet associated with pyridyl protons (*u* and *v*) are clearly resolved in this spectrum, at 7.71 and 7.64 ppm, respectively, not overlapping with any other resonances. The [Ru·**2**$_2$]$(PF_6)_2$ complex was prepared in an identical manner and so was the Ni(II) complex [Ni·**1**$_2$]$(PF_6)_2$, using $NiCl_2 \cdot xH_2O$ as the metal source. The d^8 Ni(II) ion is paramagnetic, hence the signals in the ^{1}H-NMR (600 MHz, CD_3CN) spectrum were broadened and shifted. One signal was shifted as far downfield as 56.46 ppm. All three of these complexes were observed in MALDI HRMS and their recorded isotopic distribution patterns matched calculated ones (see ESI).

The formation of the monoleptic complex [Ir·**1**Cl_3] was achieved using conditions modified from those previously reported by Collin *et al.* for analogous terpy ligands (heating under microwave irradiation to 160 °C in $(CH_2OH)_2$ for 20 minutes).[35] This complex showed very poor solubility in a range of solvents. However, the ^{1}H-NMR spectrum (400 MHz, DMSO-d_6) was successfully recorded in a dilute solution (**Fig. 1(d)**). This complex was found not to be stable and was shown to decompose over a period two weeks. It was also shown to dissociated rapidly in DMSO solution. Though not stable, it is the first example of an Ir(III)-**btp** complex to be reported to date.

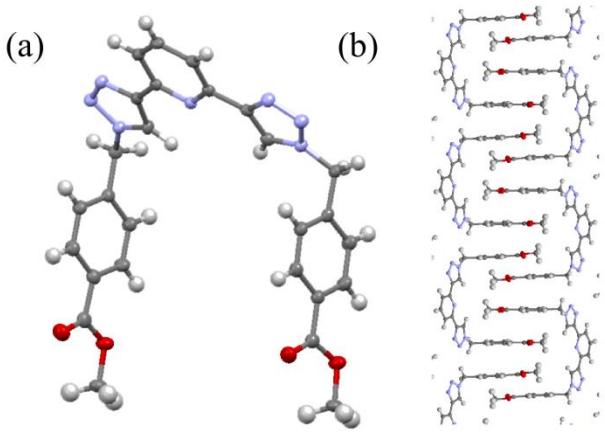

Fig. 2 (a) Crystal structure of **1** shown with thermal ellipsoids at 50% probability. Hydrogen atom positions were calculated; (b) The 'interlocking' packing structure of the ligand in the solid state.

Monoleptic Pt(II) complexes of both **1** and **2** were successfully obtained by reaction of the relevant ligand with *cis*-$[PtCl_2(DMSO)_2]$ (^{1}H-NMR spectra and HRMS of both Pt(II) complexes are shown in ESI). The ^{1}H-NMR spectrum of [Pt·**1**Cl]Cl (400 MHz, DMSO-d_6) is shown in **Fig. 1(e)**. Unlike the spectra of the other complexes, there were no overlapping resonances; the triplet arising from the 4-pyridyl proton (marked *v* in **Fig. 1**) being shifted further downfield than the other pyridyl protons (*u* in **Fig. 1**). The [Pt·**1**Cl]Cl complex was found to have limited solubility in most common solvents and it was shown to dissociate in DMSO solution over short time.

X-ray crystal structure analysis

A number of crystal structures were obtained for the complexes formed above, the general crystallographic data and structure refinements being provided in Table 1. Single crystals of **1** were grown by slow evaporation of a solution in $CHCl_3$, yielding yellow plate-like crystals, from which the solid-state X-ray structure was determined at 108 K. The ligand crystallised in the low-symmetry triclinic space group P−1. The molecule, as displayed in **Fig. 2(a)**, adopted a 'horseshoe' configuration, which is in keeping with the *anti-anti* conformation shown by Tornøe *et al*. for a structurally similar a **btp** ligand.[13]. This is a result of electrostatic repulsion between the lone pairs of the pyridyl and 3-triazolyl nitrogen atoms; resulting in the triazolyl protons pointing into the cavity. Moreover, the plane of the **btp** motif was approximately orthogonal to the planes of the phenyl rings (88.29° and 88.38°). The molecules pack in an interdigitated manner (**Fig. 2(b)**) as a result of π–π interactions between the phenyl rings in the ligand's 'arms'. The planar **btp** motifs are also arranged parallel to each other. Moreover, hydrogen-bonding interactions between three of the four methylene CH protons with triazolyl nitrogen atoms as well as an interaction of the 5-pyridyl CH with the triazolyl nitrogen, are also observed. These interactions are all of the order of 2.59(5) Å in length and at angles of 162(4)° (Details of these interactions are shown in ESI).

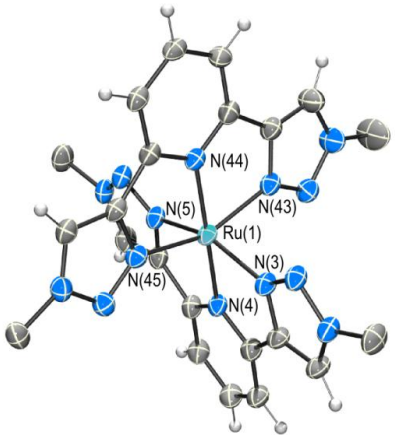

Fig. 3 Coordination sphere of $[Ru{\cdot}\mathbf{2}_2]PF_6Cl$ with thermal ellipsoids at 50% probability. Ligand 'arms', solvents and counterions have been omitted to more clearly show the atoms of interest. The **btp** motifs are arranged in a pseudo-octahedral geometry about the Ru(II) centre. Angles and bond lengths are given in Table 2. Full structure is shown in **Fig. 4**.

Table 1 Selected crystallographic data and structure refinements

Compound	**1**	$[Ru{\cdot}\mathbf{2}_2]PF_6Cl(CH_3CN)(H_2O)_{0.50}(EtOH)_{1.25}(Et_2O)_{0.50}$	$[Ni{\cdot}\mathbf{1}_2]PF_6Cl(H_2O)(CH_3CN)$	$[Ir{\cdot}\mathbf{1}Cl_3](H_2O)_{0.25}(C_2H_6O_2)_{0.25}$
Formula	$C_{27}H_{23}N_7O_4$	$C_{56.50}H_{54.50}ClF_6N_{15}O_{10.25}PRu$	$C_{56}H_{51}ClF_6N_{15}NiO_9P$	$C_{27.50}H_{25}Cl_3IrN_7O_{4.75}$
CCDC code	956219	956220	956222	956221
Formula weight	509.52	1398.14	1317.25	808.07
T (K)	108(2)	108(2)	108(2)	100(2)
Crystal system	Triclinic	Triclinic	Triclinic	Monoclinic
Space group	P−1	P−1	P−1	$P2_1/c$
a (Å)	6.3501(13)	12.235(2)	14.4083(10)	15.4149(18)
b (Å)	12.965(3)	17.491(4)	14.8238(11)	14.1809(19)
c (Å)	14.859(3)	17.627(4)	16.2001(12)	15.627(2)
α (°)	92.45(3)	105.76(3)	108.541(3)	90
β (°)	101.17(3)	105.52(3)	91.506(3)	105.781(9)
γ (°)	100.30(3)	93.49(3)	115.862(3)	90
V (Å^3)	1176.9(4)	3461.4(12)	2896.2(4)	3287.2(7)
Z	2	2	2	4
F(000)	532	1421	1356	1620
D_c (Mg·m^{-3})	1.438	1.333	1.510	1.673
μ (mm^{-1})	0.101	0.367	1.952	10.497
GOF on F^2	1.214	1.103	1.039	1.072
R_1 [I>2σ(I)]	0.0639	0.0705	0.0497	0.0470
wR_2 [I>2σ(I)]	0.1262	0.2099	0.1257	0.1226

Cite this: DOI: 10.1039/c0xx00000x

www.rsc.org/xxxxxx

ARTICLE TYPE

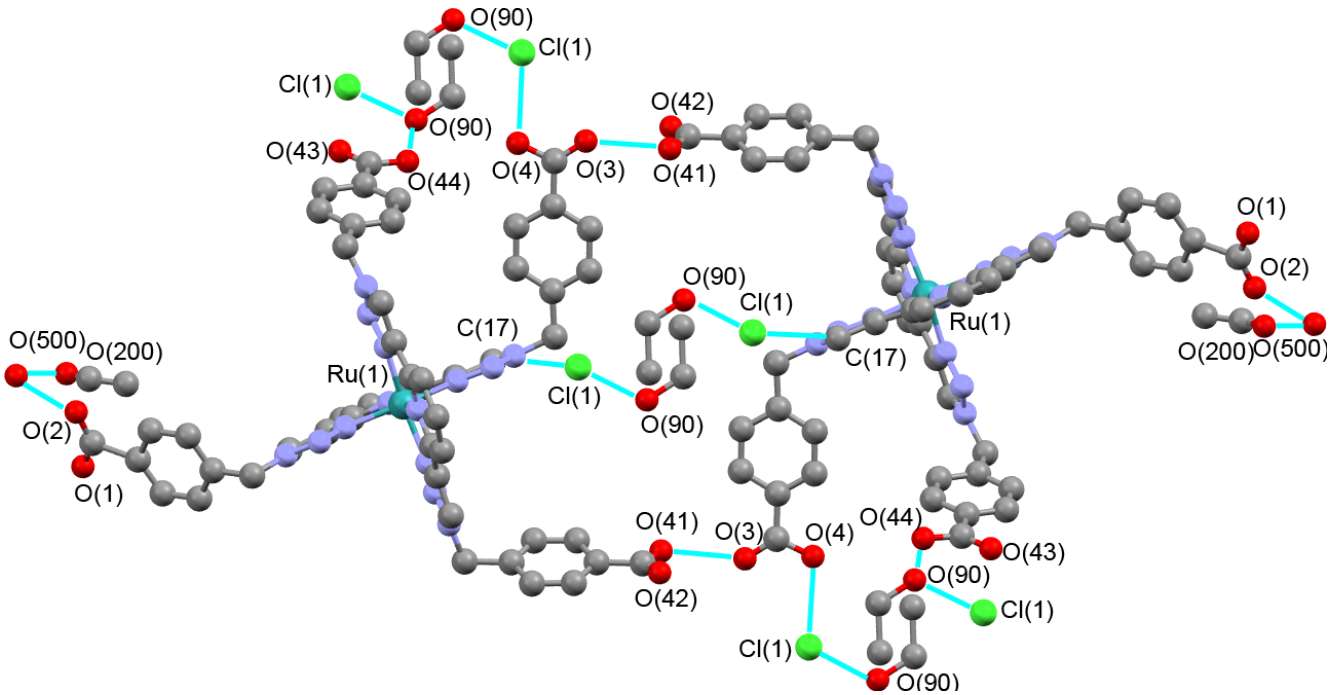

Fig. 4 A ball and stick model of the X-ray crystal structure of [Ru·**2**$_2$]PF_6Cl, showing hydrogen-bonding interactions. Uninvolved molecules of CH_3CN and Et_2O and PF_6^- counterion as well as hydrogen atoms are omitted for clarity.

Yellow crystals of complex [Ru·**2**$_2$](PF_6)Cl were grown by diffusion of diethyl ether into CH_3CN. The [Ru·**2**$_2$](PF_6)Cl crystallised in the triclinic space group P−1. When compared with the structure of ligand **1**, the triazole rings have rotated, with the N(3), N(5), N(43) and N(45) atoms coordinating the Ru(II) ion (see **Fig. 3**). The Ru(II) adopts an N6 coordination sphere and is distorted significantly from an octahedral geometry. The angle formed between the pyridyl nitrogen atoms and the Ru(II) centre is only slightly distorted at 176.5°, while the intraligand triazolyl N–Ru–N angles are all approximately 157°; deviating significantly from the ideal of 180°. The distances between the pyridyl nitrogen atoms and the Ru(II) centre are slightly shorter than those between the triazolyl nitrogen atoms and the metal. Selected bond lengths and angles between the coordinating nitrogen atoms and the Ru(II) centre are shown in Table 2. The mean planes of the two coordinating ligands' **btp** motifs were nearly orthogonal, at an angle of 87.99°. This geometry is broadly in agreement with bond angles and lengths reported for similar **btp** structures previously reported,[12,25] and also much like the geometry of the well-studied [Ru(terpy)$_2$]$(PF_6)_2$.[36] Similarly to the terpy analogue, the pyridyl N–Ru bond lengths are shorter than the triazolyl N–Ru distances. However, the difference between these two measurements is less significant than for terpy with variations of less than 0.06 Å, as opposed to nearly 0.10 Å. The angles are also more distorted from octahedral than the terpy analogue by approximately 2° in each case and the

Table 2 Selected bond lengths [Å], angles [°] and distortion parameters [°] for Ru(II), Ni(II) and Ir(III) complexes and their terpy analogues

	[Ru·**2**$_2$]PF_6Cl	[Ru(terpy)$_2$]$(PF_6)_2$[a]	[Ni·**1**$_2$]PF_6Cl	[Ni(terpy)$_2$]$(ClO_4)_2$·H_2O[b]		[Ir·**1**Cl_3]	[Ir(terpy)Cl_3][c]
M(1)-N(4)	2.021(4)	1.974(7)	2.046(2)	2.024(8)	Ir(1)-N(4)	1.996(5)	1.927(3)
M(1)-N(44)	2.023(4)	1.981(7)	2.036(2)	1.984(9)	Ir(1)-N(3)	2.057(5)	2.044(3)
M(1)-N(3)	2.051(4)	2.065(7)	2.088(2)	2.146(11)	Ir(1)-N(5)	2.022(5)	2.049(3)
M(1)-N(43)	2.051(4)	2.076(6)	2.122(2)	2.116(10)	Ir(1)-Cl(3)	2.3543(18)	2.370(1)
M(1)-N(5)	2.057(4)	2.065(6)	2.078(2)	2.113(11)	Ir(1)-Cl(1)	2.3559(17)	2.3556(7)
M(1)-N(45)	2.078(4)	2.067(6)	2.132(2)	2.108(10)	Ir(1)-Cl(2)	2.3585(17)	2.3466(8)
N(4)-M(1)-N(44)	176.50(14)	178.8(3)	175.43(8)	177.4(6)	N(4)-Ir(1)-Cl(2)	175.83(16)	177.34(8)
N(3)-M(1)-N(5)	156.79(15)	158.4(3)	154.31(8)	156.1(4)	N(3)-Ir(1)-N(5)	159.3(2)	161.3(1)
N(43)-M(1)-N(45)	156.60(15)	159.1(2)	154.24(8)	155.3(4)	Cl(3)-Ir(1)-Cl(1)	179.27(6)	179.51(3)
Σ[d]	102.5	93.3	121.4	107.0		52.1	44.4

[a] Data from Lashgari *et al.*[36] [b] Data from Rae *et al.*[37] [c] Data from Sheldrick and co-workers.[38] [d] Distortion parameter $\Sigma=\Sigma|(90°-\theta)|$ for *cis*-N–M–N angles.

Cite this: DOI: 10.1039/c0xx00000x

www.rsc.org/xxxxxx

ARTICLE TYPE

Table 3 Hydrogen bonds for [Ru·$\mathbf{2}_2$]PF_6Cl [Å and °].

D–H···A	d(D–H)	d(H···A)	d(D···A)	∠(DHA)
O(2)-H(2X)···O(200)	0.85	2.40	3.26(4)	179.0
O(111)-H(11X)···O(100)	0.92	2.62	3.390(19)	141.3
O(41)-H(41)···O(3)	0.84	1.93	2.766(6)	172.9
O(4)-H(4X)···Cl(1)	0.90	2.08	2.980(4)	176.8
O(44)-H(44X)···O(90)	0.91	1.68	2.573(6)	165.2
O(44)-H(44X)···O(90)	0.91	1.68	2.573(6)	165.2
O(200)-H(200)···O(2)	0.85	2.57	3.26(4)	137.4
O(90)-H(90X)···Cl(1)	0.86	2.18	3.048(6)	178.6
C(17)-H(17)···Cl(1)	0.95	2.857	3.589(5)	134.7

distortion parameter, Σ,[39] for this structure (equal to the sum of the deviations of each *cis*-N–Ru–N angle from the ideal of 90°) is 102.5°, which is more distorted from the ideal than the terpy structure, for which Σ is 93.3°, *cf.* Table 2.

The 'arms' of each ligand were arranged differently as shown in **Fig. 4**, with all of the terminal carboxylic acid groups being involved in hydrogen bonding in the solid state. One carboxylic group CO(1)O(2)H hydrogen bonds to a water molecule HO(500)H, which in turn hydrogen bonds to an ethanol molecule (O(200)). The two ligands show intermolecular hydrogen bonding between CO(4)O(3)H and CO(42)O(41)H with a donor–acceptor distance O(41)···O(3) measuring 2.766(6) Å. O(4) also interacts with the Cl^- counterion (O(4)-H(4X)···Cl(1) = 2.980(4) Å, 176.8°). CO(43)O(44)H hydrogen bonds to the hydroxyl group (O(90)) of one disordered ethanol molecule, which also shows interactions with the Cl^- ion, leading to a repeatable coordination network. Triazolyl C(17)H displays an interaction with Cl(1) which will be discussed in more detail below. Selected hydrogen bonding distances and angles are shown in Table 3.

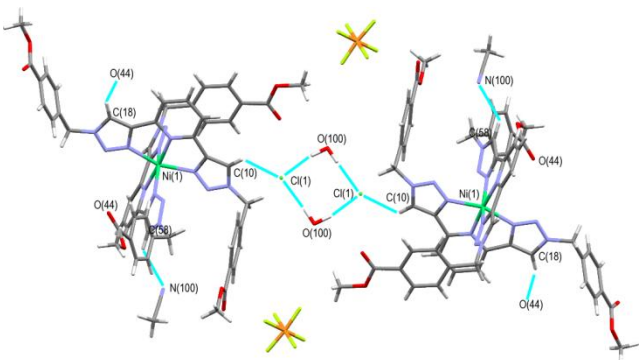

Fig. 5 Capped stick model of the packing structure of [Ni·$\mathbf{1}_2$]PF_6Cl.

A crystal structure of [Ru·$\mathbf{1}_2$]$(PF_6)_2$ in the triclinic space group P−1 was also obtained. The data was, however, not of sufficient quality to fully resolved, but clear connectivity could be ascertained, and picture of this structure is shown in the ESI (**Fig. S22**). The coordination sphere about the Ru(II) ion clearly had similar pseudo-octahedral geometry to that discussed above. However, the 'arms' were uninfluenced by any intermolecular interactions, with two distinct conformations of the complex being present in the unit cell.

Lilac crystals of the Ni(II) complex of ligand **1** were obtained upon ether diffusion into a CH_3CN solution. The [Ni·$\mathbf{1}_2$]PF_6Cl complex also crystallised in the triclinic space group P−1 with one molecule in the asymmetric unit. The structure has a distorted octahedral geometry around the metal centre, with *cis*-N–Ni–N bond angles ranging from 77.15(8)°–106.93(8)° and *trans*-N–Ni–N angles ranging from 154.24(8)°– 175.43(8)°. This structure is more distorted from octahedral geometry than the [Ru·$\mathbf{2}_2$]PF_6Cl structure, with a distortion parameter of 121.4°. The comparison of this structure to a terpy analogue (Table 2), showed that the geometry is significantly more distorted from octahedral, the average pyridyl N–Ni bond lengths are slightly longer and the average triazolyl N–Ni bonds are slightly shorter (2.105 Å compared to 2.121 Å for terpy).[37] The distortion parameter of the terpy structure is also lower, with a value of 107.0°. The packing of the [Ni·$\mathbf{1}_2$]PF_6Cl complex is shown in **Fig. 5**. In contrast to the carboxylic acid 'arms' in the structure of [Ru·$\mathbf{2}_2$]PF_6Cl above, the methyl ester ligand 'arms' of ligand **1** do not have any hydrogen bonding interactions with each other. Both hydrogen atoms of the interstitial water molecule display hydrogen bonding interactions to the chloride ions in the structure (O(100)–H···Cl(1) = 3.193(2) and 3.221(3) Å, ∠(O(100)–H···Cl(1)) = 169.3 and 169.6°), while the chloride also interacts with one of triazolyl protons C(10)H (*vide infra*). There is also a solvent···π interaction between the water molecule and N(7) of one of the triazole ringsThe lone pair on O(100) of the water molecule points towards the ring. This interaction has an O···centroid distance of 3.297 Å. Selected bond lengths and angles are provided in ESI.

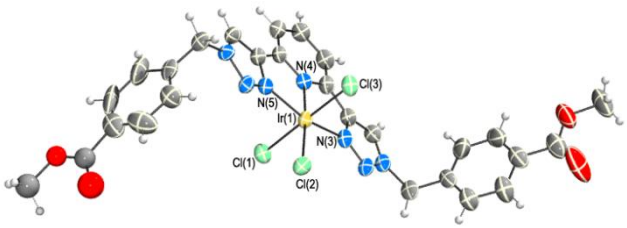

Fig. 6 X-ray crystal structure of [Ir·$\mathbf{1}Cl_3$]. Thermal ellipsoids at 50% probability. Selected bond lengths and angles are shown in Table 2.

Small single crystals of the [Ir·$\mathbf{1}Cl_3$] complex were grown by vapour diffusion of diethyl ether solution into a DMF solution. [Ir·$\mathbf{1}Cl_3$] crystallised in the monoclinic space group $P2_1/c$ with one molecule in the asymmetric unit as shown in **Fig. 6**. The structure contains one quarter occupancy ethylene glycol and one quarter occupancy water molecule. One of the ester groups was disordered over two sites with relative occupancies of 50% for each site disorder, only one position is shown in **Fig. 6** and full refinement details are provided in the ESI. The Ir(III) adopts a distorted octahedral geometry, with an N_3Cl_3 coordination sphere. The intraligand triazolyl *trans*-N–Ir–N angle, much like the

structures already discussed, is distorted from purely octahedral geometry by 159.3(2)°. The pyridyl N–Ir distance (1.996(5) Å) was shorter than the triazolyl N–Ir distances (2.057(5) and 2.022(5) Å). The bond lengths and angles in the complexes are comparable to those in an analogous terpy structure as shown in Table 2.[38] Comparison of the distortion parameters for both structures shows that [Ir·**1**Cl_3] is more distorted (Σ = 52.1°) from pure octahedral than the terpy analogue (Σ = 44.4°). No crystals of the Pt(II) complexes suitable for X-ray crystallography were obtained; this was due mostly to the poor solubility of these complexes in most common solvents.

The structures of the three complex [Ru·**2**$_2$]PF_6Cl, [Ni·**1**$_2$]PF_6Cl and [Ir·**1**Cl_3] all displayed non-classical hydrogen bonding interactions between the acidic triazole CH and chloride ions present in the structures, Table 4. As well as binding cations, such as *d*-block metals, it has been shown that 1,2,3-triazole ligands are capable of recognising anions. Anion receptors have been reported which take advantage of these interactions, either to simultaneously bind both metal ions and halide from salts such as KCl,[41] encapsulate chloride ions in the cavity of a macrocycle,[42] or template the formation of interlocked structures.[43] Despite their potential for interesting interactions, however, triazole C–H···Cl^- bonds have not been widely investigated, but studies published with structural data consistently report donor–acceptor distances of the order of 3.5 Å.[44-45] The bond lengths and angles for the C–H···Cl^- bonds in our structures (as shown in Table 4) are very similar to each other, with H···Cl^- distances of 2.6–2.8 Å and with donor–acceptor distances being between 3.3–3.6 Å. The Cl^- being located about 134° out of the plane of the C–H bond in all cases. Having structurally characterised the aforementioned complexes, we next investigated the supramolecular properties of [Ru·**2**$_2$]$^{2+}$.

Table 4 Non-classical hydrogen bond lengths [Å] and angles [°] for all three complexes. (D=donor, A=acceptor)

Metal	D-H···A	d(D-H)	d(H···A)	d(D···A)	∠(DHA)
Ru(II)	C(17)-H(17)···Cl(1)	0.950	2.857	3.589(5)	134.7
Ni(II)	C(10)-H(10A) ··Cl(1)	0.950	2.7042	3.434(3)	134.1
Ir(III)	C(18)-H(18A) ··Cl(2)	0.950	2.623	3.358(8)	134.4

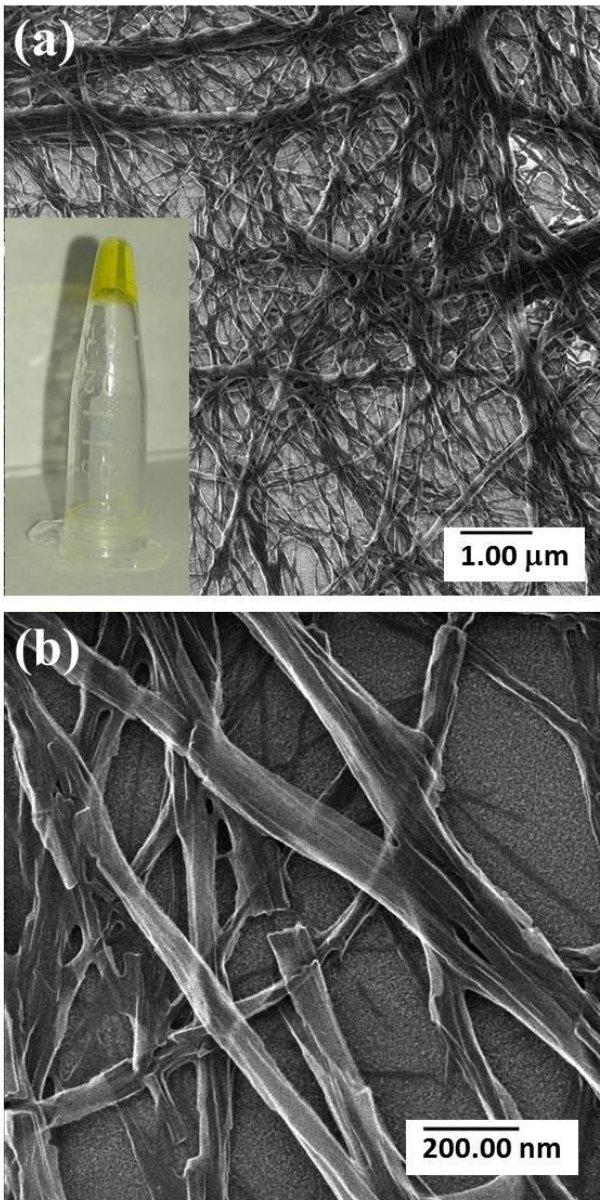

Fig. 7 HIM images of Ru(II) gel (a, b) showing its fibrous microstructure. The inset in (a) shows the formation of the metallogel in ethanol.

Formation of supramolecular metallogels

The structural analysis of [Ru**2**$_2$]PF_6Cl discussed above (**Fig. 4**) suggests the potential of this compound for the formation of supramolecular metallogels due to the presence of polymer chains within its crystal structure through hydrogen bond interactions between the carboxylic groups and chloride anions. There currently exists a great interest within the field of supramolecular and materials chemistry in the search for such new materials with various functional properties that are different from their monomeric components.[46] We have recently shown the use of lanthanide ions for the formation of luminescent organic metallogels (or supramolecular gels) and self-assembly Langmuir-Blodget films.[47] The former we have recently shown can be used as a matrix for the growth of inorganic salt nanowires (*e.g.* NaCl, KCl and KI)[48] while others have used this idea to create optically healable supramolecular polymers[49] or potential luminescent reporters for micro-environmental changes.[50]

Here the supramolecular metallogel of [Ru**2**$_2$]PF_6Cl was formed in several steps by preparing an ethanol solution of the dichloride complex followed by addition of a saturated aqueous solution of NH_4PF_6 with subsequent formation of a precipitate (the bis-(PF_6) complex). The supranatant was then decanted off and left to stand overnight resulting in the formation of viscous yellow soft material, which was identified as gel by simple "inversion test".[51] The gel exhibited luminescence similar to that of the ligand (*vide infra*). ^{1}H-NMR (400MHz, DMSO-d_6) and HRMS confirmed that the gel contained [Ru·**2**$_2$]$^{2+}$ (**Fig. S7 and S15** in ESI).

The fibrous nature of the gels was revealed by scanning electron microscopy (SEM) (see ESI) and helium ion (HIM) microscopy (**Fig. 7**). Both analyses showed similar structure of the material but HIM allowed us to obtain higher quality data compared to SEM. We believe that fibres consists of Ru(II) complexes connected together through hydrogen bonding

Cite this: DOI: 10.1039/c0xx00000x

www.rsc.org/xxxxxx

ARTICLE TYPE

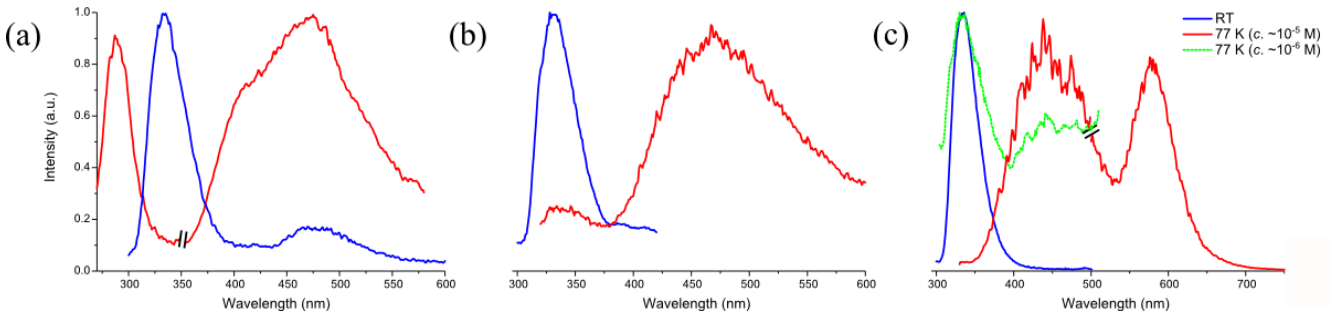

Fig. 8 Emission spectra of (a) [Ru·**1**Cl_2(DMSO)], (b) [Ir·**1**Cl_3] and (c) [Pt·**1**Cl]Cl at room temperature (blue) and 77 K (red). In (a) and (c), the spectrum is cut where a different filter had to be applied. In (c) the green trace is the emission spectrum of glass at 77 K with concentration of ~10^{-6} M.

forming in a similar manner to the network found by structural analysis (**Fig. 4**) involving carboxylic groups, chloride anions and solvent molecules. The average width of the fibres was found to be in a range of 100±25 nm; where the secondary order arrangement of the fibres can be found under higher magnification with a width of 20±5 nm (**Fig. 7(b)**). Structural analysis of any of the other *d*-metal complexes investigated in this work did not suggest the formation of supramolecular metallogels; and this was in deed verified as the attempts to obtain similar materials for them was on all occasion, not successful. However, simple structural modification of these ligands by for instance, incorporating large polymer chains, or other functional groups either at the central pyridyl unit or on the arms themselves, or be simply employing coordination with other metal ions, such as the *f*-metal ions, or the use of mixed transition and lanthanide metal ions, would open up an avenue for the creation of new materials with various functional properties, such as luminescent and magnetic properties, and we are currently investigating these avenues of research in a greater detail using such structural analogues of **1** and **2**.

Photophysical investigations

Having structurally characterised the Ru(II) and Ir(III) complexes of **1** and **2**, we next investigated their various physical properties, and that of the ligands; beginning by investigating their photophysical properties since both Ru(II) and Ir(III) complexes, in particular, are often found to possess desirable luminescence. The same properties for the [Ru·**1**Cl_2(DMSO)], [Pt·**1**Cl]Cl and [Pt·**2**Cl]Cl, complexes (for which X-ray crystal structures was not obtained), were also investigated in a similar manner.

All the photophysical properties were investigated in spectroscopic grade CH_3CN solution. The UV-Vis absorbance spectrum of ligand **1** at room temperature displayed two bands with maxima at 235 nm (ε 45031 L mol^{-1} cm^{-1}) and 300 nm (ε 8705.5 L mol^{-1} cm^{-1}) upon excitation of this ligand, a broad emission band centred at 335 nm was observed. This band exhibited a lifetime of ~2.5 ns. Ligand **2** had almost identical spectroscopic behaviour (see ESI).

The absorbance spectrum of [Ru·**1**$_2$]$(PF_6)_2$ in CH_3CN showed bands similar to those of the ligand, but blue-shifted, only slightly in the case of the band centred at 232 nm, but by ~15 nm for the band at 286 nm, the band associated with the binding triazoles. The spectrum also exhibits a new MLCT band at 395 nm.

Bis-terdentate Ru(II) complexes (including $[Ru(terpy)_2]^{2+}$) are often practically non-luminescent, due to thermal population from their ^{3}MLCT excited states to a close-lying non-emitting metal centred (MC) excited states. It has been reported that modifying the ligand structures can, however, raise the energy of the MC state and hence, increase the luminescence arising from such structurally modified complex. Perfect octahedral geometry about the metal ion is thought to increase the MC energy by leading to a strong ligand field.[52] However, as it has been shown in the structural studies above that the coordination environment in these complexes is distorted significantly from pure octahedral geometry (Σ = 102.5°), we did not necessarily expect [Ru·**1**$_2$]$(PF_6)_2$ to be highly luminescent in solution. Indeed, as has been the case with most **btp**-based ligands as well as simple terpy-based ligands, [Ru·**1**$_2$]$(PF_6)_2$ showed no long-lived luminescence at room temperature, as only a ligand-centred fluorescence band at 335 nm ($\tau \approx 2.5$ ns) similar to that of the ligand was observed. Moreover, degassing the solution led to only a slight enhancement of luminescence intensity; confirming the above. The excitation spectrum observed was also similar to that of the ligand. In light of this, luminescence emission spectra of [Ru·**1**$_2$]$(PF_6)_2$ were also recorded at 77 K, but unfortunately, no emission was observed. Similarly, for the spectroscopic properties of [Ru·**2**$_2$]$(PF_6)_2$ were found to follow the almost identical path; [Ru·**1**$_2$]$(PF_6)_2$ only giving rise to very week luminesce (see ESI). A sample of the metallogel derived from this species was immobilised on a quartz slide and the solid state luminescence measured at room temperature, and as had been seen for both the [Ru·**1**$_2$]$(PF_6)_2$ and [Ru·**2**$_2$]$(PF_6)_2$, complexes, only ligand-centred emission (centred at 310 nm) was observed for the metallogel (see ESI **Fig. S32**).

Monoleptic complex [Ru·**1**Cl_2(DMSO)] had quite different properties to that seen above. The absorbance bands recorded for [Ru·**1**Cl_2(DMSO)] were centred at 230, 302, 354 and 450 nm and the [Ru·**1**Cl_2(DMSO)] displayed an emission centred at 335 nm as well as a very broad but significantly less intense luminescence at with its maximum at 475 nm, upon excitation at high energy.

At 77 K, the emission was however, found to be centred at 285 nm with a broad band of comparable intensity being also observed at longer wavelengths; being centred at 475 nm.

The absorbance profile of [Ir·**1**Cl_3] displayed a band at 232 nm with a shoulder at 260 nm. A band centred at 293 nm tailed off until 480 nm. At room temperature, there was a luminescence band observed at 330 nm, while at 77 K, a broad luminescence centred at 450 nm became much more apparent; the fluorescence band at 335 nm being seen as a shoulder in the spectrum.

Planar Pt(II) complexes have been reported to have complicated emission behaviour, particularly at low temperature, as a result of the potential for stacking in solution, leading to Pt(II)–Pt(II) interactions, as well as interactions between the aromatic ligands;[31] the emission spectra for complexes such as $[Ru(terpy)Cl]^+$ being known to vary with concentration as well. In the case of [Pt·**1**Cl]Cl a broad absorbance profile was observed in CH_3CN, with a sharp maximum at 222 nm and tailing to 400 nm. At room temperature, only the ligand centred emission was observed for [Pt·**1**Cl]Cl, being centred at 333 nm. However, when recorded in CH_3CN glasses (concentration of ~10^{-5} M) at 77 K, two broad emission bands were observed at 442 nm and 578 nm, for [Pt·**1**Cl]Cl. Bands of similar energies have been assigned to π-π* emission and interligand π-π interactions respectively for the analogous terpy complex.[31] More dilute glasses (concentration of ~10^{-6} M) show a ligand centred emission band at 335 nm as well as a weakly structured emission around 450 nm. This emission spectrum closely resembles the spectra for the other monoleptic complexes discussed above. Complex [Pt·**2**Cl]Cl displayed similar photophysical behaviour with concentrated glasses displaying emission at 460 and 572 nm and at lower concentrations, two overlapping bands at 340 and 355 nm, the details being given in the ESI.

Electrochemistry

In addition to photophysical properties, the electrochemical properties of transition metal complexes such as those above, are regularly studied. The electrochemistry of the Ru(II) complexes was investigated by cyclic voltammetry in CH_3CN solution. Both the [Ru·**1**$_2$]$(PF_6)_2$ and [Ru·**2**$_2$]$(PF_6)_2$ showed fully reversible metal-centred oxidation of Ru(II) to Ru(III) at a potential of 1.42 V *vs* SCE (Saturated calomel electrode). Variation of the ligand 'arms' from 4-(methylcarboxy)benzyl to 4-(carboxy)benzyl had almost no impact on the donor properties of the chelating ligand, which is in agreement with the remote location of these functional groups and their similar electronic impact. The oxidation potentials are higher than those reported for terpy-type complexes, *e.g.* +1.30 (*vs* SCE) for $[Ru(terpy)_2](PF_6)_2$,[53] which may be a direct consequence of the five- *vs* six-membered peripheral heterocycles and the ensuing better mutual alignment of metal coordination axes and the lone pairs in the terpy system. While a related $[Ru(\mathbf{btp})_2]^{2+}$ complex with alkyl substituents at the triazole units featured a redox behaviour similar to $[Ru(terpy)]^{2+}$,[12] Hecht and co-workers reported very similar oxidation potentials to those observed here for a **btp** complex with 4-iodophenyl 'arms' ($E_{1/2}$ = +1.06 *vs* Fc/Fc^+, that is, +1.46 V *vs* SCE).[25] This similarity suggests a minor influence of the triazole substituent on the metal oxidation potential, which is in agreement with the weaker orbital alignment between **btp** and the octahedral ruthenium centre as compared to terpy-type systems. As expected, neutral [Ru·**1**Cl_2(DMSO)] was much easier oxidised ($E_{1/2}$ = +0.75) than the cationic complexes. The CH_3CN oxidation potential is slightly higher than that reported for the and CH_3NO_2 were identical, (shown in ESI†) suggesting that potential solvent exchange reactions due to the coordinating nature of CH_3CN are irrelevant. [Ir·**1**Cl_3] showed no oxidation up to solvent discharge potential.

Table 5 Half-wave potentials and anodic–cathodic peak separations of redox curves for Ru(II) complexes.

Complex	$E_{1/2}$ [V]	ΔE_p [mV]
[Ru·**1**$_2$]$(PF_6)_2$	+1.42[a]	70
[Ru·**2**$_2$]$(PF_6)_2$	+1.42[a]	60
[Ru·**1**Cl_2(DMSO)]	+0.75[b]	58

[a] sweep rate 100 mV s^{-1}, $[NBu_4]PF_6$ as supporting electrolyte (1 mM), potentials *vs* SCE using Fc^+/Fc as internal standard ($E_{1/2}$ = +0.40 V (ΔE_p = 72 mV); [b] $[Ru(bpy)_3]^{2+}/[Ru(bpy)_3]^{3+}$ as internal standard ($E_{1/2}$ = +1.39V (ΔE_p = 55 mV)

Conclusions

In this article we have developed novel terdentate **btp** ligands **1** and **2**, by using click-chemistry. These were characterised using various spectroscopic techniques, and their behaviour with *d*-block metal ions explored. The X-ray crystal structures of ligand **1** and three of the resulting complexes, allowed investigation into coordination geometry of these ligands with Ru(II), Ni(II) and Ir(III). The coordination sphere of these structures closely resembled the distorted octahedral geometry of analogous terpy structures. The triazole rings played an important role in these structures, with the nitrogen atoms acting as hydrogen bond acceptors and the CH acting as a hydrogen bond donor.

The three complexes showed non-classical triazolyl C–H···Cl^- hydrogen bonding interactions with C–H···Cl^- distances of 3.364(6)–3.589(5) Å and bond angles of 134°. The photophysical behaviour of these complexes in solution was also studied; and only the ligand-centred fluorescence was observed at room temperature for all complexes except [Ru·**1**Cl_2(DMSO)]. Low temperature studies showed no emission for the dileptic complex, and a broad band centred at ~450 nm for each of the monoleptic complexes [Ru·**1**Cl_2(DMSO), [Ir·**1**Cl_3] and [Pt·**1**Cl]Cl. Concentrated glasses of [Pt·1Cl]Cl and [Pt·2Cl]Cl showed new emission bands consistent with stacking behaviour. Electrochemical measurements of Ru(II) complexes showed that these compounds had higher oxidation potentials than similar and analogous compounds in the literature.

The X-ray crystal structure of complex $[Ru\cdot\mathbf{2}_2]^{2+}$ showed an extensive hydrogen-bonding network involving the carboxylic acid 'arms' of the ligand, chloride anions and solvent molecules. This complex was shown to form gels in EtOH solution and microscopy images (using both scanning electron microscopy and helium ion microscopy) of these gels showed a fibrous structure with fibre widths in the range of 100±25 nm. When immobilised on a quartz slide, this gel exhibited ligand-centred emission much like that seen for the complex in solution. Such systems suggest a vast potential for application as materials with various functions including surface healing or oxidation–reduction response, and we are investigating these at present.

Experimental

General methods and materials

All chemicals were purchased from commercial sources and unless specified used without further purification. Melting points were determined using an Electrothermal IA9000 digital melting point apparatus. Elemental analysis was carried out at the Microanalytical Laboratory, School of Chemistry and Chemical Biology, University College Dublin. Infrared spectra were recorded on a Perkin Elmer Spectrum One FT-IR Spectrometer fitted with a universal ATR sampling accessory. NMR spectra were recorded using a Bruker DPX-400 Avance spectrometer or Agilent DD2/LH spectrometer, operating at 400.13 MHz for ^{1}H-NMR, 100.6 MHz for ^{13}C-NMR, or a Bruker AV-600 spectrometer, operating at 600.1 MHz for ^{1}H-NMR and 150.2 MHz for ^{13}C-NMR. All spectra were recorded using commercially-available deuterated solvents, and were referenced to solvent residual proton signals. Electrospray mass spectra were measured on a Micromass LCT spectrometer calibrated using a leucine enkephaline standard. MALDI Q-Tof mass spectra were carried out on a MALDI Q-Tof Premier (Waters Corporation, Micromass MS technologies, Manchester, UK) and high-resolution mass spectrometry was performed using Glu-Fib as an internal reference (peak at *m/z* 1570.677). All microwave reactions were carried out in 2–5 mL or 10–20 mL Biotage Microwave Vials in a Biotage Initiator Eight EXP microwave reactor.

X-ray Crystallography

X-ray data (Table 1) were collected on either a Rigaku Saturn 724 CCD Diffractometer (for **1** and [Ru·$\mathbf{2}_2$]PF_6Cl) using graphite-monochromated Mo-Kα radiation (λ = 0.71073 Å) or a Bruker Apex2 Duo (for [Ni·$\mathbf{1}_2$]PF_6Cl and [Ir·$\mathbf{1}$$Cl_3$]) using a high intensity Cu-Kα radiation source (λ = 1.54178 Å). The data sets from the Rigaku Saturn-724 diffractometer were collected using Crystalclear-SM 1.4.0 software. Data integration, reduction and correction for absorption and polarisation effects were all performed using the Crystalclear-SM 1.4.0 software. Space group determination, was obtained using Crystalstructure ver.3.8 software. The datasets collected on the Bruker Apex2 Duo were processed using Bruker APEXv2011.8-0 software. All structures were solved by direct methods (SHELXS-97) and refined against all F^2 data (SHELXL-97) using shelXle.[55,56] All H-atoms, except for O–H protons, were positioned geometrically and refined using a riding model with d(CH_{aro}) = 0.95 Å, *U*iso = 1.2*U*eq (C) for aromatic, d(CH) = 0.99 Å, *U*iso = 1.2*U*eq (C) for CH_2 and 0.98 Å, *U*iso = 1.2*U*eq (C) for CH_3. O–H protons were found from the difference map and fixed to the attached atoms with $U_H = 1.2U_O$.

Crystallographic data for these structures has been deposited with the Cambridge Crystallographic Data Centre, (CCDC, 12 Union Road, Cambridge CB21EZ, UK; http://www.ccdc.cam.ac.uk). Copies can be obtained free of charge on quoting the deposition numbers 956219-956222.

Microscopy studies of the gels

To image the gel samples by scanning electron microscopy (SEM), they were deposited manually onto clean silicon samples with a thick silicon dioxide layer. The spatula and glass pipettes used for dosing and silicon pieces used as substrates were all cleaned thoroughly by sonication in HPLC grade acetone followed by HPLC grade propan-2-ol. The gels were manually drop cast on to the silicon at room temperature and dried during 5 days at ambient conditions. Low kV SEM was carried out using the Zeiss ULTRA Plus using either an SE2 or in-lens detector and the Zeiss Orion Plus Helium Ion Microscope using an SE2 detector, both in the Advanced Microscopy Laboratory, CRANN, Trinity College Dublin. The samples prepared for the imaging did not have any additional conductive layer cover. Beam energies for the helium ion were 30-35 kV with probe currents ranging from 0.1–1.5 pA. A 10 μm beam limiting aperture was employed for all the images. Images were formed by collecting the secondary electrons generated during the helium ion interacting with the specimen atoms. Charge control was achieved using an electron flood gun. After each line scan charge neutralisation was applied. The image was acquired using either 32 or 64 line averaging.

Cyclic voltammetry

Electrochemical studies were carried out using a Metrohm Autolab Potentiostat Model PGSTAT101 employing a gastight three electrode cell under an argon atmosphere. A platinum disk with 7.0 mm^2 surface area was used as the working electrode and polished before each measurement. The reference electrode was Ag/AgCl, the counter electrode was a Pt foil. In all experiments Bu_4NPF_6 (0.1 M in dry CH_3CN) was used as supporting electrolyte with analyte concentrations of approximately 1 mM. The ferrocenium/ferrocene redox couple was used as an internal reference ($E_{1/2}$ = 0.40 V vs. SCE).[57]

Photophysical measurements

UV-Visible absorbance spectra were measured in 1 cm quartz cuvettes on a Varian Cary 50 spectrophotometer. Baseline correction was applied for all spectra. Emission spectra were measured on a Varian Cary Eclipse luminescence spectrometer. All the stock solutions were prepared in CH_3CN.

Some emission spectra were also recorded on a Fluorolog FL-3−22 spectrometer from Horiba-Jobin-Yvon Ltd. A Jobin Yvon FluoroHub single photon counting controller fitted with an appropriate wavelength Jobin Yvon NanoLED was used to measure lifetimes, which were determined from the observed decays using DataStation v2.4.

Syntheses of ligands and metal ion complexes

2,6-Bis((trimethylsilyl)ethynyl)pyridine (3). Protected bis-alkyne **3** was prepared from 2,6-dibromopyridine by Sonogashira coupling using a modified literature procedure.[58,59] The reaction mixture was stirred at room temperature under argon atmosphere for 24 hours, using a dry 1:1 Et_3N:THF solvent system. The solution was diluted with ethyl acetate and stirred vigorously with a solution of EDTA/NH_4OH for 1 hour. The reaction mixture was then extracted with ethyl acetate and washed with saturated $NaHCO_3$ solution and brine before drying over $MgSO_4$ and concentrating under reduced pressure, yielding a brown solid. Crude product was filtered through a silica plug, washing in hexane/CH_2Cl_2 (1:1) and the eluent concentrated under reduced pressure, yielding **3** as a tan coloured solid (3.10 g, 11.410 mmol, 68%). m.p. 90.3–98.7 °C (Lit. m.p. 97–99 °C).[60] HRMS (*m/z*) (ESI^+): Calculated for $C_{15}H_{22}NSi_2^+$ *m/z* = 272.1291 $[M+H]^+$.

Found *m/z* = 272.1299; ^{1}H NMR (400 MHz, $CDCl_3$): δ = 0.28 (s, 18H, TMS), 7.41 (d, 2H, *J* = 7.8 Hz, 3- and 5-pyridyl CH), 7.62 (t, 1H, *J* = 7.8 Hz, 4-pyridyl CH); IR ν_{max} (cm^{-1}): 3052 (strong), 2962, 2900, 2154 (C≡C), 1558, 1440, 1249, 1206, 1163, 1082, 985, 953, 836, 811 (strong), 759, 734, 702, 656.

General procedure for synthesis of btp ligands 1 and 2

To a solution of the relevant bromide (4.65 mmol) in 15 mL DMF/water (4:1) was added sodium azide (0.332 g, 4.65 mmol) and the reaction mixture stirred for 1 hour, yielding the azide derivative, which was not isolated, and therefore used without further purification.** To this solution was added **3** (0.631 g, 2.33 mmol). $CuSO_4{\cdot}5H_2O$ (0.232 g, 0.93 mmol) and sodium ascorbate (0.368 g, 1.86 mmol) were added to the reaction mixture, followed by anhydrous K_2CO_3 (0.650 g, 4.70 mmol) and stirred at room temperature for 18 hours in a further 15 mL 4:1 DMF/water. EDTA/NH_4OH solution was added to the reaction mixture and stirred for 1 hour before isolating the product.

2,6-Bis(1-(4-(methylcarboxy)benzyl)-1,2,3-triazol-4-yl)pyridine (1). Ligand **1** was prepared according to the general procedure above from methyl 4-(bromomethyl)benzoate and was isolated upon extraction with $CHCl_3$, washing the organic layer with brine. Concentration under reduced pressure and trituration with cold CH_3OH followed by recrystallisation from boiling CH_3OH yielded ligand **1** as an off-white solid (1.27 g, 2.49 mmol, 53%). m.p. 221.1–223.5 °C. HRMS (*m/z*) (ESI^+): Calculated for $C_{27}H_{23}N_7O_4Na^+$ *m/z* = 532.1709 $[M+Na]^+$. Found *m/z* = 532.1711; Calculated for $C_{27}H_{23}N_7O_4$, C = 63.65, H = 4.55, N = 19.24. Found C = 63.38 H = 4.52 N = 19.29. ^{1}H NMR (400 MHz, DMSO): δ = 3.84 (s, 6H, $–OCH_3$), 5.81 (s, 4H, CH_2), 7.45 (d, 4H, *J* = 8.2 Hz, Ph CH), 7.91–8.07 (m, 7H, Ph CH and pyr CH), 8.72 (s, 2H, triazolyl CH); ^{13}C NMR (150 MHz, $CDCl_3$): δ = 52.4 ($–OCH_3$), 53.8 (CH_2), 119.4 (3- and 5-pyridyl CH), 122.1 (triazolyl CH), 127.8 (phenyl CH), 130.3 (phenyl CH), 130.6 (qt, phenyl), 137.8 (4-pyridyl CH), 139.3 (qt, phenyl), 148.8 (qt, triazolyl), 149.7 (qt, 2- and 6-pyridyl), 166.3 (C=O). IR ν_{max} (cm^{-1}): 3154, 3078 (ar C–H st), 3010, 2956 (C–H st), 2845 (O–CH_3 st), 2101, 1729 (C=O st), 1608 and 1572 (C–C γ), 1511, 1436, 1426, 1314, 1278, 1236, 1214, 1196, 1155, 1109, 1085, 1044, 1022, 991, 973, 843, 820, 797, 782, 756, 732, 687, 667.

2,6-Bis(1-(4-(carboxy)benzyl)-1,2,3-triazol-4-yl)pyridine (2). Like **1** above, carboxylic acid ligand **2** was synthesised from 4-(bromomethyl) benzoic acid. It was isolated upon acidification of the EDTA/NH_4OH solution by dropwise addition of concentrated HCl solution until pH 7 was reached. **2** was collected as a beige solid upon suction filtration (0.705 g, 1.46 mmol, 63%). Product decomposed over 284 °C. HRMS (*m/z*) (ESI^-): Calculated for $C_{25}H_{18}N_7O_4^-$ *m/z* = 480.1426 $[M–H]^-$. Found *m/z* = 480.1423; Calculated for $C_{25}H_{19}N_7O_4{\cdot}0.5H_2O$, C = 57.46, H = 3.86, N = 18.76. Found C = 57.39, H = 3.75, N = 18.92. ^{1}H NMR (600 MHz, DMSO): δ (ppm) = 5.80 (s, 4H, CH_2), 7.45 (d, 4H, *J* = 8.7 Hz, Ph CH), 7.91–8.03 (m, 7H, Ph CH and pyr CH), 8.74 (s, 2H, triazolyl CH); ^{13}C NMR (150 MHz, DMSO-d_6): δ (ppm) = 52.8 (CH_2), 118.7 (3- and 5-pyr CH), 124.1 (triazolyl CH), 128.2 (phenyl CH), 129.9 (Ph CH), 130.6 (Ph qt), 138.1 (4-pyr CH), 140.8 (Ph qt), 147.5 (triazolyl qt), 149.8 (2- and 4-pyr qt), 167.03 (C=O); IR ν_{max} (cm^{-1}): 3083 (ar C–H st), 2938 (C–H st), 1719, 1692 (C=O st), 1642, 1614, 1531, 1467, 1420, 1400, 1285, 1242, 1198, 1176, 1106, 1047, 942, 822, 800, 725.

Monoleptic Ru(II) complex ([Ru·1Cl$_2$(DMSO)]). Precursor *cis*-$[RuCl_2(DMSO)_4]$ was prepared in a microwave reaction according to a literature procedure from $RuCl_3xH_2O$.[61] To this complex (0.029 g, 0.059 mmol) was added the ligand **1** (0.030 g, 0.059 mmol) and 5 mL $CHCl_3$ and the mixture refluxed in darkness for 10 hours before isolating the product complex upon filtration and washing with ether, yielding a bright red solid (0.039 g, 0.051 mmol, 86%). Product decomposed over 216 °C. HRMS (*m/z*) (MALDI): Calculated for $C_{27}H_{23}N_7O_4Cl_2Ru^+$ *m/z* = 681.0232 $[M–(DMSO)]^+$. Found *m/z* = 681.0213; Calculated for $C_{29}H_{29}N_7O_5SRuCl_2{\cdot}0.5CHCl_3$, C = 43.25, H = 3.63, N = 11.97. Found C = 43.60, H = 3.39, N = 11.83; ^{1}H NMR (600 MHz, DMSO-d_6): δ (ppm) = 3.49 (s, 6H, coordinated DMSO), 3.86 (s, 6H, $–OCH_3$), 5.92 (s, 4H, CH_2), 7.54 (d, 4H, Ph CHs, *J* = 8.0 Hz), 8.01 (d, 4H, Ph CHs, *J* = 8.0 Hz), 8.07–8.18 (m, 3H, pyr CH), 9.16 (s, 2H, triazolyl CH); ^{13}C NMR (150 MHz, DMSO-d_6): δ = 46.8 (coordinated DMSO), 52.6 ($–OCH_3$), 54.3 (CH_2), 119.0 (pyr CH), 125.7 (triazolyl CH), 128.9 (Ph CH), 130.1 (Ph CH), 137.8 (pyr CH), 140.2 (qt), 149.9 (qt), 150.9 (qt), 166.1 (qt); IR ν_{max} (cm^{-1}): 3443 (br), 3011, 2925, 1715 (strong), 1614, 1580, 1418, 1283 (strong), 1185, 1108 (strong), 1085, 1018, 993, 961, 931, 809, 749, 718, 677.

General procedure for synthesis of dileptic Ru(II) and Ni(II) complexes. To the relevant ligand (2 equiv.) was added 5 mL aqueous ethanol solution (70% v/v). The solution was degassed and $RuCl_3{\cdot}xH_2O$ or $NiCl_2{\cdot}xH_2O$ (1 equiv.) added. This was stirred for 40 minutes at 120 °C under microwave irradiation. The yellow reaction mixture was filtered through celite and concentrated under reduced pressure. Ethanol was added to solubilise the complex before centrifuging. The supernatant was decanted off and a few drops of NH_4PF_6 were added before centrifuging again. The solution was decanted off and the solid which had formed was dissolved in CH_3CN and concentrated under reduced pressure, yielding a solid.

Dileptic Ru(II) complex of 1 ([Ru·1$_2$](PF$_6$)$_2$). Complex $[Ru{\cdot}\mathbf{1}_2](PF_6)_2$ was prepared according to the general procedure for dileptic complexes outlined above, from ligand **1** (0.056 g, 0.11 mmol) and $RuCl_3{\cdot}xH_2O$ (0.012 g, 0.05 mmol), yielding a bright yellow solid (0.015 g, 0.01 mmol, 28%). This was dissolved in CH_3CN and crystallised *via* ether diffusion. m.p. 236.1–238.0 °C. HRMS (*m/z*) (MALDI): Calculated for $C_{54}H_{46}N_{14}O_8F_6PRu^+$ *m/z* = 1265.2308 $[M–PF_6]^+$. Found *m/z* = 1265.2323; Calculated for $C_{54}H_{46}N_{14}O_8F_{12}P_2RuNa^+$ *m/z* = 1433.1848. Found *m/z* = 1433.1832. $[M+Na]^+$; Calculated for $C_{54}H_{46}N_{14}O_8RuP_2F_{12}{\cdot}3H_2O$, C = 44.30, H = 3.58, N = 13.39. Found C = 44.22, H = 3.17, N = 13.39; ^{1}H NMR (600 MHz, DMSO-d_6): 3.75 (s, 6H, $–OCH_3$), 5.35 (s, 4H, CH_2), 6.62 (d, 4H, *J* = 7.0 Hz, Ph CH), 7.18 (d, 4H, *J* = 7.0 Hz, Ph CH), 7.64 (t, 1H, *J* = 6.9 Hz, 4-pyr CH), 7.71 (d, 2H, *J* =6.8 Hz, 3- and 5-pyr CH), 8.41 (s, 2H, triazolyl CH); ^{13}C NMR (150 MHz, DMSO-d_6): δ (ppm) = 52.6 ($–OCH_3$), 54.5 (CH_2), 120.8 (4-pyr CH), 127.2 (triazolyl CH), 128.4 (Ph CH), 130.0 (Ph CH), 138.4 (3-, 5-pyr

CH), 139.4 (Ph qt), 150.3 (triazolyl qt), 165.9 (carbonyl qt); ^{19}F NMR (376 MHz, DMSO-d_6): δ = −70.6 (d, J = 706.1 Hz, PF_6); ^{31}P NMR (162 MHz, DMSO-d_6): δ = −142.98 (apparent quin, J = 711.4 Hz); IR ν_{max} (cm^{-1}): 3322, 1711, 1640, 1618, 1572, 1646, 1428, 1281, 1191, 1111, 828 (strong), 730.

Dileptic Ru(II) complex of 2 ([Ru·2$_2$](PF$_6$)$_2$). Complex [Ru·**2**$_2$](PF$_6$)$_2$ was prepared according to the general procedure for dileptic complexes outlined above, using dicarboxylate **2** (0.100 g, 0.21 mmol) and $RuCl_3{\cdot}xH_2O$ (0.023 g, 0.11 mmol), yielding a bright yellow solid (0.069 g, 0.06 mmol, 26%). This was re-dissolved in a 1:1 mixture of CH_3CN and ethanol and crystallised *via* ether diffusion. A large yellow crystal was formed and structure determined by X-ray diffractometry. m.p. 206.5–209.6 °C. HRMS (*m/z*) (MALDI): Calculated for $C_{50}H_{37}N_{14}O_8Ru^+$ *m/z* = 1063.1962 [M−2(PF$_6$)−H]+ . Found *m/z* = 1063.1998; Calculated for $C_{50}H_{38}N_{14}O_8RuP_2F_{12}{\cdot}3H_2O$, C = 42.65 H = 3.15 N = 13.93. Found C = 42.05 H = 2.58 N = 13.70; ^{1}H NMR (400 MHz, DMSO-d_6): δ = 5.67 (s, 8H, CH_2), 7.19 (d, 8H, J = 8.3 Hz, Ph CH**),** 7.86 (d, 8H, J = 8.2 Hz, Ph CH), 8.36 (t, 2H, J = 7.7 Hz, 4-pyr CH), 8.45 (d, 4H, J = 7.7 Hz, 3- and 5-pyr CH), 9.26 (s, 4H, triazolyl CH); ^{13}C NMR (150 MHz, DMSO-d_6): δ = 53.8 (CH_2), 120.0 (3-, 5-pyr CH), 126.3 (triazolyl CH), 127.7 (Ph CH), 129.7 (Ph CH), 131.0 (Ph qt), 137.5 (4-pyr CH), 137.8 (Ph qt), 149.0 (pyr qt), 149.5 (triazolyl qt), 166.3 (C=O qt); ^{19}F NMR (376 MHz, DMSO-d_6): δ = −70.6 (d, J = 711.4 Hz, PF_6); ^{31}P NMR (162 MHz, DMSO-d_6): δ = −142.99 (apparent quin, J = 711.2 Hz); IR ν_{max} (cm^{-1}): 3321, 2921, 2850, 1695, 1615, 1576, 1421, 1261, 1111, 1056, 1020, 805 (strong).

Ni(II) complex of 1 ([Ni·1$_2$](PF$_6$)$_2$). Complex [Ni·**1**$_2$](PF$_6$)$_2$ was prepared according to the general procedure outlined above using **1** (0.100 g, 0.20 mmol) and $NiCl_2{\cdot}xH_2O$ 0.013 g, 0.10 mmol). Ether diffusion into a CH_3CN solution yielded lilac needle-like crystalline solid (0.020 g, 0.014 mmol, 20%). m.p. 189.9–193.8 °C; HRMS (*m/z*) (MALDI+): Calculated for $C_{54}H_{46}N_{14}O_8NiF_6P^+$ *m/z* = 1221.2618. Found *m/z* = 1221.2644; Calculated for $C_{54}H_{46}N_{14}O_8NiP_2F_{12}{\cdot}H_2O$, C = 46.81, H = 3.49, N = 14.15. Found C = 46.83, H = 2.98, N = 13.78; ^{1}H NMR (600 MHz, CD_3CN): δ = 3.84 (br), 5.49 (br), 6.41 (br), 7.86 (br), 17.48 (br), 29.94 (br), 56.46 (br); ^{13}C NMR (150 Hz, CD_3CN, assigned by CH COSY): δ = 50.2, 126.2; ^{19}F NMR (376 MHz, CD_3CN): δ = −73.4 (d, J = 706.6 Hz, PF_6); ^{31}P NMR (162 MHz, CD_3CN): δ = −144.6 (apparent quin, J = 706.4 Hz, PF_6); IR ν_{max} (cm^{-1}): 3077, 2615, 2301, 1714 (strong), 1615, 1592, 1579, 1512, 1474, 1435, 1419, 1316, 1279 (strong), 1217, 1183, 1110 (strong), 1065, 1053, 1020, 967, 813 (strong), 770, 726 (strong), 619, 604, 589, 576, 555 (strong).

Ir(III) Complex of 1 ([Ir·1Cl$_3$]). Complex [Ir·**1**Cl$_3$] was synthesised using a modified literature procedure.[35,62] Ligand **1** (0.210 g, 0.41 mmol) and $IrCl_3{\cdot}xH_2O$ (0.130 g, 0.41 mmol) were suspended in ethylene glycol (5 mL). The reaction mixture was degassed before heating at 160 °C in darkness for 20 minutes under microwave irradiation. The reaction mixture was allowed to cool to room temperature before filtering to collect precipitate. The precipitate was washed with ethanol, H_2O and Et_2O, yielding complex [**1**·IrCl$_3$] as a yellow solid (0.166 g, 0.21 mmol, 50%). Product decomposed over 330 °C. HRMS (*m/z*) (ESI$^+$): Calculated for $C_{27}H_{23}N_7O_4Cl_3IrNa^+$ *m/z* = 830.0404 [M+Na]$^+$. Found *m/z* = 830.0373; Calculated for $C_{27}H_{23}N_7O_4IrCl_3{\cdot}C_2H_6O_2$, C = 40.03, H = 3.36, N = 11.27. Found C = 39.37, H = 3.05, N = 10.99; ^{1}H NMR (400 MHz, DMSO-d_6): δ = 3.86 (s, 6H, $-OCH_3$), 6.08 (s, 4H, CH_2), 7.61 (d, 4H, J = 8.4 Hz, phenyl CH), 8.05 (d, 4H, J = 8.2 Hz, Ph CH), 8.15 (t, 1H, J = 7.7 Hz, 4-pyr CH), 8.30 (d, 2H, J = 7.8 Hz, 3- and 5-pyr CH), 9.33 (s, 2H, triazolyl CH); ^{13}C NMR (150 MHz, DMSO-d_6, assigned from CH COSY): δ = 52.7 ($-OCH_3$), 55.2 (CH_2), 120.4 (3-, 5-pyr CH), 127.5 (triazolyl CH), 129.2 (Ph CH), 130.2 (Ph CH), 141.1 (4-pyr CH); IR ν_{max} (cm^{-1}): 3498, 3124, 2955, 1723 (strong), 1615, 1594, 1478, 1431 (strong), 1349, 1277 (strong), 1219, 1187, 1110 (strong), 1085, 1074, 1052, 1022, 953, 869, 807, 770, 753, 726 (strong), 713, 687, 658, 634, 622.

General procedure for preparation of Pt(II) complexes. Precursor *cis*-[PtCl$_2$(DMSO)$_2$] was prepared from K$_2$[PtCl$_4$] according to a literature procedure and used without further purification.[63] To this complex (1 equiv.) was added ligand **1** or **2** (1 equiv.) and the suspension refluxed in CH_3OH in darkness for 5 hours. The reaction mixture was cooled over ice before isolation of the product.

Pt(II) complex of 1 ([Pt·1Cl]Cl). According to the general procedure above, ligand **1** (0.081 g, 0.16 mmol) was treated with *cis*-[PtCl$_2$(DMSO)$_2$] (0.069 g, 0.16 mmol). Product was purified by filtering the reaction mixture, concentrating the filtrate, re-dissolving this in $CHCl_3$ and centrifuging. The supranatent was decanted off and the process repeated until the supranatent was colourless. The resultant yellow solid was the pure complex [Pt·**1**Cl]Cl (0.024 g, 0.032 mmol, 20%). Product decomposed over 250 °C. HRMS (*m/z*) (ESI$^+$): Calculated for $C_{27}H_{23}N_7O_4ClPt^+$ *m/z* = 739.1148 [M−Cl]$^+$. Found *m/z* = 739.1143; Calculated for $C_{27}H_{23}N_7O_4PtCl_2{\cdot}0.5H_2O$, C = 39.55 H, = 2.84, N = 11.74. Found C = 40.07, H = 2.42, N = 11.70; ^{1}H NMR (400 MHz, DMSO-d_6): δ = 3.83 (s, 6H, $-OCH_3$), 6.00 (s, 4H, CH_2), 7.57 (d, 4H, J = 8.3 Hz, Ph CH), 8.01 (d, 4H, J = 8.3 Hz, Ph CH), 8.22 (d, 2H, J = 8.0 Hz, 3, 5-pyr CH), 8.47 (t, 1H, J = 8.1 Hz, 4-pyr CH), 9.32 (s, 2H, triazolyl CH); IR ν_{max} (cm^{-1}): 3423, 3076, 2953, 1716 (strong), 1614, 1595, 1579, 1512, 1479, 1434, 1418, 1313, 1280 (strong), 1223, 1184, 1110 (strong), 1074, 1047, 1019, 965, 840, 812, 747, 725 (strong), 687, 659.

Pt(II) complex of 2 ([Pt·2Cl]Cl). According to the general procedure above, **2** (0.183 g, 0.38 mmol) was treated with *cis*-[PtCl$_2$(DMSO)$_2$] (0.161 g, 0.38 mmol). Product was isolated upon filtration and washed with CH_3OH, $CHCl_3$ and Et_2O, yielding [Pt·**2**Cl]Cl as a yellow solid (0.212 g, 0.298 mmol, 78%). Product decomposed over 350 °C HRMS (MALDI): Calculated for $C_{25}H_{19}N_7O_4ClPt^+$ *m/z* = 711.0835 [M−Cl]$^+$. Found *m/z* = 711.0859; Calculated for $C_{25}H_{19}N_7O_4PtCl_2{\cdot}1.5CHCl_3$, C = 34.35, H = 2.23, N = 10.58. Found C = 34.02, H = 2.01, N = 10.33; ^{1}H NMR (600 MHz, CD_3OD): δ (ppm) = 5.96 (s, 4H, CH_2), 7.65 (d, 4H, J = 8.3 Hz, Ph CH), 8.06–8.18 (m, 6H, Ph CH and 3-, 5-pyr CH), 8.39 (t, 1H, J = 8.2 Hz, 4-pyr CH), 9.13 (s, 2H, triazolyl CH); ^{13}C NMR (150 MHz, CD_3OD): δ = 55.7 (CH_2), 120.5 (3- and 5-pyr CH), 127.1 (triazolyl CH), 128.4 (Ph CH), 130.1 (Ph

CH), 131.5 (qt), 142.3 (4-pyr) CH, 148.1 (qt), 151.3 (qt), 151.7 (qt), 167.3 (C=O qt); IR ν_{max} (cm^{-1}): 3424, 3077, 2635, 1698 (strong), 1614, 1580, 1480, 1419, 1388, 1279 (strong), 1182, 1116 (strong), 1073, 1049, 1017, 818 (strong), 752 (strong), 729 (strong).

Acknowledgements

We thank the Irish Research Council Embark Initiative (Postgraduate Postgraduate Scholarship JPB, and Postdoctoral Fellowship to JAK) and Science Foundation Ireland for financial support (SFI 2010 and 2012 Principal Investigation grants (TG and JJB, respectively). JPB would like to thank Dr Jennifer E. Jones, Dr Steve Comby, Samuel Bradberry, Bryan Hogan, Colm Delaney and Dr Gearóid Ó Máille for useful discussion. We would like to thank Dr John O'Brien for technical assistance and useful discussion of NMR results and Prof. Sylvia Draper for use of low-temperature spectroscopy apparatus.

Notes and references

[a] *School of Chemistry and Trinity Biomedical Sciences Institute, Trinity College, Pearse St, Dublin 2, Ireland. Fax: +353 1 716 2628; Tel: +353 1 896 3459; E-mail: gunnlaut@tcd.ie*

[b] *School of Chemistry & Chemical Biology, University College Dublin, Belfield, Dublin 4, Ireland.*

[c] *School of Chemistry and Centre for Research on Adaptive Nanostructures and Nanodevices (CRANN), Trinity College Dublin, Dublin 2, Ireland.*

[d] *Chemistry, Faculty of Natural & Environmental Sciences, University of Southampton, Highfield, Southampton, SO17 1BJ, United Kingdom*

† Electronic Supplementary Information (ESI) available. Selected ^{1}H-NMR spectra, HRMS isotopic patterns of complexes, crystallographic tables and supplementary images, microscopy images, photophysical spectra and CV spectra. See DOI: 10.1039/b000000x/

‡ As well as '**btp**', this motif has been referred to as '**tripy**' in the work of Professor Ulrich Schubert and co-workers.

***Safety comment*: sodium azide is very toxic. Organic azides are potentially explosive and care must be taken in their handling.

1. R. B. P. Elmes, M. Erby, S. A. Bright, D. C. Williams and T. Gunnlaugsson, *Chem. Commun.*, 2012, **48**, 2588-2590.
2. R. B. P. Elmes, K. N. Orange, S. M. Cloonan, D. C. Williams and T. Gunnlaugsson, *J. Am. Chem. Soc.*, 2011, **133**, 15862-15865.
3. T. Gunnlaugsson, S. Banerjee, J. A. Kitchen, S. Bright, J. E. O'Brien, D. C. Williams and J. M. Kelly, *Chem. Commun.*, 2013, DOI:10.1039/c3cc44962a.
4. a) R. B. P. Elmes, J. A. Kitchen, D. C. Williams, and T. Gunnlaugsson, *Dalton Trans.*, 2012, **41**, 6607–6610. b) A. M. Nonat, S. J. Quinn and T.Gunnlaugsson, *Inorg. Chem.* 2009, **48**, 4646. c) G. J. Ryan, S. Quinn and T. Gunnlaugsson, *Inorg. Chem*. 2008, **47**, 401. d) M. Wojdyla, J. A. Smith, S. Vasudevan, S. J. Quinn and J. M. Kelly, *Photochem. Photobiol. Sci.* 2010, **9**, 1196. e) M. J. Hannon, P. S. Green, D. M. Fisher, P. J. Derrick, J. L. Beck, S. J. Watt, S. F. Ralph, M. M. Sheil, P. R. Barker, N. W. Alcock, R. J. Price, K. J. Sanders, R. Pither, J. Davis and A. Rodger, *Chem. Eur. J.*, 2006, **12**, 8000-8013.
5. A. Alshehri, P. Beale, J. Q. Yu and F. Huq, *Anticancer Res.*, 2010, **30**, 4547-4553.
6. T. Kinoshita, J. T. Dy, S. Uchida, T. Kubo and H. Segawa, *Nature Photonics*, 2013, **7**, 535-539.
7. F. S. Han, M. Higuchi, T. Ikeda, Y. Negishi, T. Tsukuda and D. G. Kurth, *J. Mater. Chem.*, 2008, **18**, 4555-4560.
8. a) J. A. Kitchen, E. M. Boyle and T. Gunnlaugsson, *Inorg. Chim. Acta*, 2012, **381**, 236-242. b)P. Wang, Z. Li, G.-C. Lv, H.-P. Zhou, C. Hou, W.-Y. Sun and Y.-P. Tian, *Inorg. Chem. Commun.*, 2012, **18**, 87-91. c) A. M. Nonat, A. J. Harte K. Senechal-David, J. P. Leonard and T. Gunnlaugsson, *Dalton Trans.*, 2009, 4703.
9. R. M. Meudtner, M. Ostermeier, R. Goddard, C. Limberg and S. Hecht, *Chem. Eur. J.*, 2007, **13**, 9834-9840.
10. L. Munuera and R. K. O'Reilly, *Dalton Trans.*, 2010, **39**, 388-391.
11. T. El Malah, S. Rolf, S. M. Weidner, A. F. Thünemann and S. Hecht, *Chem. Eur. J.*, 2012, **18**, 5837-5842.
12. Y. Li, J. C. Huffman and A. H. Flood, *Chem. Commun.*, 2007, 2692-2694.
13. P. Danielraj, B. Varghese and S. Sankararaman, *Acta Crystallogr. Sect. C*, 2010, **66**, m366-m370.
14. C. W. Tornøe, C. Christensen and M. Meldal, *J. Org. Chem.*, 2002, **67**, 3057-3064.
15. V. V. Rostovtsev, L. G. Green, V. V. Fokin and K. B. Sharpless, *Angew. Chem. Int. Ed.*, 2002, **41**, 2596-2599.
16. T. R. Chan, R. Hilgraf, K. B. Sharpless and V. V. Fokin, *Org. Lett.*, 2004, **6**, 2853-2855.
17. J. K. Molloy, O. Kotova, R. D. Peacock and T. Gunnlaugsson, *Org. Biomol. Chem.*, 2012, **10**, 314-322.
18. J. D. Crowley and P. H. Bandeen, *Dalton Trans.*, 2010, **39**, 612-623.
19. B. Schulze, C. Friebe, M. D. Hager, A. Winter, R. Hoogenboom, H. Gorls and U. S. Schubert, *Dalton Trans.*, 2009, 787-794.
20. B. Schulze, C. Friebe, S. Hoeppener, G. M. Pavlov, A. Winter, M. D. Hager and U. S. Schubert, *Macromol. Rapid Commun.*, 2012, **33**, 597-602.
21. Y. Li, M. Pink, J. A. Karty and A. H. Flood, *J. Am. Chem. Soc.*, 2008, **130**, 17293-17295.
22. E. Brunet, O. Juanes, L. Jiménez and J. C. Rodríguez-Ubis, *Tetrahedron Lett.*, 2009, **50**, 5361-5363.
23. J. Yuan, X. Fang, L. Zhang, G. Hong, Y. Lin, Q. Zheng, Y. Xu, Y. Ruan, W. Weng, H. Xia and G. Chen, *J. Mater. Chem.*, 2012, **22**, 11515-11522.
24. C. Zhang, X. Shen, R. Sakai, M. Gottschaldt, U. S. Schubert, S. Hirohara, M. Tanihara, S. Yano, M. Obata, N. Xiao, T. Satoh and T. Kakuchi, *J. Polym. Sci., Part A: Polym. Chem.*, 2011, **49**, 746-753.
25. M. Ostermeier, M.-A. Berlin, R. M. Meudtner, S. Demeshko, F. Meyer, C. Limberg and S. Hecht, *Chem. Eur. J.*, 2010, **16**, 10202-10213.
26. B. Schulze, D. Escudero, C. Friebe, R. Siebert, H. Görls, U. Köhn, E. Altuntas, A. Baumgaertel, M. D. Hager, A. Winter, B. Dietzek, J. Popp, L. González and U. S. Schubert, *Chem. Eur. J.*, 2011, **17**, 5494-5498.
27. B. Schulze, D. Escudero, C. Friebe, R. Siebert, H. Görls, S. Sinn, M. Thomas, S. Mai, J. Popp, B. Dietzek, L. González and U. S. Schubert, *Chem. Eur. J.*, 2012, **18**, 4010-4025.
28. J. A. G. Williams, A. J. Wilkinson and V. L. Whittle, *Dalton Trans.*, 2008, 2081-2099.
29. B. Schulze, C. Friebe, S. Hoeppener, G. M. Pavlov, M. D. Hager, A. Winter and U. S. Schubert, *Polym. Prepr.*, 2011, **52**, 917-918.
30. K. M.-C. Wong and V. W.-W. Yam, *Coord. Chem. Rev.*, 2007, **251**, 2477-2488.
31. J. A. Bailey, M. G. Hill, R. E. Marsh, V. M. Miskowski, W. P. Schaefer and H. B. Gray, *Inorg. Chem.*, 1995, **34**, 4591-4599.
32. R. M. Meudtner and S. Hecht, *Macromol. Rapid Commun.*, 2008, **29**, 347-351.
33. J. T. Fletcher, B. J. Bumgarner, N. D. Engels and D. A. Skoglund, *Organomet.*, 2008, **27**, 5430-5433.
34. J. T. Fletcher, S. E. Walz and M. E. Keeney, *Tetrahedron Lett.*, 2008, **49**, 7030-7032.
35. J.-P. Collin, I. M. Dixon, J.-P. Sauvage, J. A. G. Williams, F. Barigelletti and L. Flamigni, *J. Am. Chem. Soc.*, 1999, **121**, 5009-5016.
36. K. Lashgari, M. Kritikos, R. Norrestam and T. Norrby, *Acta Crystallogr. Sect. C*, 1999, **55**, 64-67.
37. A. T. Baker, D. C. Craig and A. D. Rae, *Aust. J. Chem.*, 1995, **48**, 1373-1378.
38. M. Dobroschke, Y. Geldmacher, I. Ott, M. Harlos, L. Kater, L. Wagner, R. Gust, W. S. Sheldrick and A. Prokop, *ChemMedChem*, 2009, **4**, 177-187.
39. J. Nelson, V. McKee and G. Morgan, in *Prog. Inorg. Chem.*, John Wiley & Sons, Inc., 2007, 10.1002/9780470166482.ch2, pp. 167-316.
40. A. Spek, *Acta Crystallogr. D*, 2009, **65**, 148-155.
41. S. C. Picot, B. R. Mullaney and P. D. Beer, *Chem. Eur. J.*, 2012, **18**, 6230-6237.
42. Y. Li and A. H. Flood, *Angew. Chem. Int. Ed.*, 2008, **47**, 2649-2652.

43. N. G. White and P. D. Beer, *Chem. Commun.*, 2012, **48**, 8499-8501.
44. a) Y. Hua and A. H. Flood, *Chem. Soc. Rev.*, 2010, **39**, 1262-1271. b)Y. Li and A. H. Flood, *J. Am. Chem. Soc.*, 2008, **130**, 12111-12122
45. L. Brammer, E. A. Bruton and P. Sherwood, *Cryst. Growth Des.*, 2001, **1**, 277-290.
46. a) J. Zhang and C.-Y.Su, *Coord. Chem. Rev*., 2013, **257**, 1373-1408; b) A. Y.-Y Tam and V. W.-W.Yam *Chem. Soc. Rev*., 2013, **42**, 1540-1567. c) M.-O. M. Piepenbrock, G. O. Lloyd, N. Clarke and J. W. Steed, *Chem. Rev.*, 2009, **110**, 1960-2004.
47. a) O. Kotova, R. Daly, C. M. G. dos Santos, M. Boese, P. E. Kruger, J. J. Boland and T. Gunnlaugsson, *Angew. Chem. Int. Ed.*, 2012, **51**, 7208-7212. b) J. A. Kitchen, D. E. Barry, L. Mercs, M. Albrecht, R.D. Peacock, and T. Gunnlaugsson, *Angew. Chem. Int. Ed*. 2012, **51**, 704 –708. c) D. E. Barry, J. A. Kitchen, M. Albrecht, S. Faulkner, and T. Gunnlaugsson, *Langmuir*, 2013, **29**, DOI: 10.1021/la402274s.
48. a) R. Daly, O. Kotova, M. Boese, T. Gunnlaugsson and J. J. Boland, *ACS Nano*, 2013, **7**, 4838-4845.
49. M. Burnworth, L. Tang, J. R. Kumpfer, A. J. Duncan, F. L. Beyer, G. L. Fiore, S. J. Rowan and C. Weder, *Nature*, 2011, **472**, 334-337.
50. a) L. Sambri, F. Cucinotta, G. De Paoli, S. Stangi, L. De Cola, *New J. Chem*. 2010, ***34***, 2093-2096. b)A. Y.-Y. Tam, K. M.-C. Wong and V. W.-W. Yam, *J. Am. Chem. Soc.*, 2009, **131**, 6253-6260.
51. M.-O. M. Piepenbrock, N. Clarke, J. W. Steed, *Langmuir*, 2009, **25**, 8451-8456.
52. J. Dinda, S. Liatard, J. Chauvin, D. Jouvenot and F. Loiseau, *Dalton Trans.*, 2011, **40**, 3683-3688.
53. T. Norrby, A. Börje, B. Åkermark, L. Hammarström, J. Alsins, K. Lashgari, R. Norrestam, J. Mårtensson and G. Stenhagen, *Inorg. Chem.*, 1997, **36**, 5850-5858.
54. R. Ziessel, V. Grosshenny, M. Hissler and C. Stroh, *Inorg. Chem.*, 2004, **43**, 4262-4271.
55. C. B. Hubschle, G. M. Sheldrick and B. Dittrich, *J. Appl. Crystallogr.*, 2011, **44**, 1281-1284.
56. G. Sheldrick, *Acta Crystallogr. Sect. A*, 2008, **64**, 112-122.
57. N. G. Connelly and W. E. Geiger, *Chem. Rev*., 1996, **96**, 877-910.
58. B. H. Dana, B. H. Robinson and J. Simpson, *J. Organomet. Chem.*, 2002, **648**, 251-269.
59. Y. Shin, G. E. Fryxell, C. A. Johnson Ii and M. M. Haley, *Chem. Mater*., 2007, **20**, 981-986.
60. J. M. Heemstra and J. S. Moore, *Org. Lett.*, 2004, **6**, 659-662.
61. A. Harvey, M. Draganjac, S. Chui, R. Snell and E. Benjamin, *Journal of the Arkansas Academy of Science*, 2009, **63**, 185.
62. L. Flamigni, J.-P. Collin and J.-P. Sauvage, *Acc. Chem. Res.*, 2008, **41**, 857-871.
63. R. Cini, A. Donati and R. Giannettoni, *Inorg. Chim. Acta*, 2001, **315**, 73-80.

Synthesis, structural, photophysical and electrochemical studies of various *d*-metal complexes of btp [2,6-bis(1,2,3-triazol-4-yl)pyridine] ligands that give rise to the formation of metallo-supramolecular gels

Joseph P. Byrne, Jonathan A. Kitchen, Oxana Kotova, Vivienne Leigh, Alan P. Bell, John J. Boland, Martin Albrecht, and Thorfinnur Gunnlaugsson

The development of two new **btp** ligands (**1** and **2**) for *d*-metal ions is described. The X-ray crystal structures of several of these complexes are presented, as well as the results of the electro and the photochemical analysis for number of these complexes. The Ru(II) complex of **2** was shown to give rise to gel formation which is due to the direct formation of supramolecular networks in ethanol solution.